Nitrogen recovery using a membrane contactor: Modelling nitrogen and pH evolution

G. Noriega-Hevia*, J. Serralta*, L. Borrás**, A. Seco**, J. Ferrer*

*CALAGUA – Unidad Mixta UV-UPV, Institut Universitari d'Investigació d'Enginyeria de l'Aigua i Medi Ambient – IIAMA, Universitat Politècnica de Valencia, Camí de Vera s/n, 46022 Valencia, Spain. guinohe@cam.upv.es; jserralt@hma.upv.es; jferrer@hma.upv.es.

**CALAGUA, Unidad Mixta UV-UPV, Departament d'Enginyeria Química, Universitat de València, Avinguda de la Universitat s/n, 46100 Burjassot, València, Spain. luis.borras-falomir@uv.es; aurora.seco@uv.es.

1. Introduction

Nitrogen present in urban wastewaters has been traditionally removed using biological processes such as nitrification (ammonium is converted into nitrite by ammonium oxidizing microorganisms, followed by transformation into nitrate via nitrite oxidizing microorganisms) and denitrification (nitrate is reduced to molecular nitrogen, which is released to the atmosphere). Although nitrogen removal from wastewaters avoids the harmful effects of nitrogen contamination of the water bodies (eutrophication, toxicity problems), it is not comply with the aims of circular economy. On the one hand, the industrial Haber-Bosch process for ammonia production is energy-intensive, consuming 6.4×10^{12} MJ/year of non-renewable energy which is equivalent to 90,000,000 cars in terms of energy usage or almost 80,000,000 people in terms of global warming potential [1]. On the other hand, nitrogen removal from wastewaters requires large amounts of energy, where the aeration for nitrification alone occupies between 50-70% of total energy consumption in wastewater treatment plants (WWTPs) [2]. A new sewage treatment paradigm based on the so-called water resource recovery facility

29   (WRRF) concept has emerged within the scientific community for waste-to-resource

30   recovery [3]. Within this paradigm, sewage is no longer considered as a waste but as a

31   source of raw valuable resources, resulting in environmental and economic benefits [4].

32   Nitrogen is one of these valuable resources present in wastewaters, which are expected

33   to be recovered.

34   Different physical, chemical and biological approaches have been developed in recent

35   decades for nitrogen recovery. Some of these approaches are problematic because they

36   produce low-purity products, present high costs, or are operationally complex. Struvite

37   ($MgNH_4PO_4 \cdot 6H_2O$) crystallization is an extensively researched approach which has

38   been implemented in different full scale WWTPs; it produces valuable products with

39   few environmental risks. Many studies have been conducted to produce struvite from

40   different wastewaters such as reject water generated from anaerobic sludge digestion

41   and dewatering processes [5], urine [6] or aquaculture wastewater [7]. However,

42   nitrogen recovery efficiency obtained in municipal WWTPs by means of struvite

43   crystallization is limited due to the equimolar stoichiometry of struvite. Struvite

44   crystallization can remove between 80-90% of PO_4^{3-} and between 20-30% of NH_4^+ [8].

45   Stripping of free ammonia involves the physical transfer of NH_3 from the aqueous phase

46   (waste stream) to a gas phase which is then transferred to an air scrubber, where mass

47   transfer and absorption of the NH_3 from the gas to a liquid phase, often sulphuric acid

48   (H_2SO_4), takes place in order to produce and recover a concentrated solution of

49   ammonium sulphate (($NH_4)_2SO4$; AmS) as an end-product. AmS is an inorganic salt,

50   which could be reused as a marketable fertilizer rich in direct available macronutrients,

51   N and S, thereby providing a valuable substitute for chemical fertilizers based on fossil

52   resources. The major technical bottlenecks observed to date in free ammonia stripping

53 are scaling and fouling of the packing material, and the consequent high energy and

54 chemical requirements [9].

55 Regarding membrane technologies, hollow fibre membrane contactors (HFMC) are a

56 promising technology for nitrogen recovery. HFMC are gas-permeable membranes in

57 hollow fibre configuration, usually made of polypropylene (PP) or

58 polytetrafluoroethylene (PTFE). In this technology, free ammonia is stripped from the

59 feed aqueous solution into gas-filled pores of the membrane on the other side of which

60 sulphuric acid reabsorbs the free ammonia producing ammonium sulphate. The

61 difference between the free ammonia concentrations on both sides of the membrane is

62 the driving force that causes the transfer of free ammonia across the membrane by

63 diffusion. By means of such a technique, large towers required for ammonia stripping

64 are replaced with small membrane devices having orders of magnitude larger surface

65 area per unit device volume. This methodology offers the prospect of being: selective to

66 ammonia removal; able to operate without the need of a big amount of energy input (as

67 in the case of air stripping); and suitable for removal of ammonium nitrogen to very low

68 levels [10].

69 Once free ammonia transfers across the hydrophobic membrane, the ammonium-

70 ammonia equilibrium on the shell side will be perturbed and as such ammonium species

71 would be expected to convert to free ammonia creating protons and reducing the

72 solution pH. Consequently, during operation of a membrane contactor for ammonia

73 recovery it may be necessary to control the solution pH at values over 8.6 by addition of

74 an appropriate alkali reagent in order to maintain the driving force for the membrane

75 separation process. pH can also be raised by aeration decreasing the operational costs of

76 this technology. Aeration enhances carbon dioxide stripping modifying the carbonate-

77 bicarbonate-carbon dioxide equilibria. Carbonate and bicarbonate are converted to

78 carbon dioxide releasing OH^- and increasing the solution pH [11].

79 HFMCs have been also applied for different porpoises [12,13]. Regarding to

80 wastewater treatment, this technology has been applied with high recovery efficiencies

81 to different nitrogen rich streams such as reject water from anaerobic sludge digestion

82 [14], swine manure [15] and landfill leachate [16]. HFMCs combined with a cost-

83 effective flow-electrode capacitive deionization unit able to concentrate ammonium

84 ions (CapAmm) have also been applied to low-loaded streams [17]. To our knowledge,

85 the first application of hollow fibre membrane contactors in full scale municipal WWTP

86 was recently reported by Ritcher et al [18]. The economic value of the AmS produced is

87 not the only benefit related to nitrogen recovery from reject water in WWTPs. The

88 reduction of the nitrogen load entering the biological treatment reduces the energy

89 consumption and the NOx emissions. It is important to highlight that the nitrification-

90 denitrification process requires over 5-6 kWh/kg-N, being one of the most energy-

91 demanding process in WWTPs [19].

92 Several mathematical models have been developed in previous studies for predicting

93 ammonia removal using HFMCs. Firstly, Wickramasinghe et al [20] analysed the effect

94 of pH, flow rates and nitrogen concentration on the mass transfer coefficient. In the

95 same way, Ashrafizadeh and Khorasani [21] ranked the influence of different

96 parameters on the mass transfer coefficient, including the presence of excess ions in the

97 ammonia feed solution. In both works, pH was established as the most influential factor

98 over the mass transfer coefficient. Furthermore, Tan et al [22] modelled the ammonia

99 removal with polyvinylidene fluoride (PVDF) membrane contactors incorporating the

100 resistance in the feed and membrane phases and a membrane post-treatment with

101 ethanol. Ethanol improves the hydrophobicity and the effective surface porosity of the

102   membrane and, subsequently, enhances the nitrogen recovery. Agrahari et al [23]

103   developed a mathematical model taking into account the molecular and Knudsen

104   diffusion effects as well as the rates of adsorption and desorption of ammonia molecules

105   to and from the walls of the pores during the transport through the membrane.

106   Furthermore, several 2D mathematical models incorporating the effect of pore diffusion

107   and mass transfer resistance have also been proposed [24,25]. Most recently, Nagy et al

108   [26] applied the membrane module of ChemCAD 7.1.4 program to simulate the

109   nitrogen recovery process. However, these complex models are not able to predict the

110   pH evolution in the feed solution. As commented before, pH in the nitrogen rich

111   solution decreases during ammonia mass transfer across the membrane reducing the

112   ammonia recovery rate being the key of the recovery process.

113   This paper presents a mathematical model able to predict the time evolution of total

114   ammonium nitrogen concentration and pH in different operating conditions. The model

115   considers that the ammonia transfer rate depends on the difference between free

116   ammonia concentrations at both sides of the membrane. Since free ammonia

117   concentration depends on total ammonium nitrogen concentration and pH and both

118   parameters varied during the process, the developed model considers the ammonia

119   stripping process jointly with all the acid-base reactions affecting the pH. The

120   mathematical model was implemented in MATLAB-Simulink and linked to

121   MINTEQA2 in order to calculate the concentration of every species present in

122   equilibrium. The developed model was validated with 26 laboratory-scale experiments

123   carried out at different operating conditions. In these experiments, the pH of the

124   nitrogen rich solution, the feed flow rate, the membrane surface and the temperature

125   was varied to evaluate the model capability to represent the effect of these parameters

126   on the ammonia recovery rate. The experiments were carried out using as nitrogen rich

127   solution the reject water obtained from a municipal wastewater treatment plant. The

128   novelty of this study lays in integrating in a mathematical model the time evolution of

129   pH and TAN concentration. The developed model is able to predict the pH decrease

130   observed during the ammonia stripping process and to determine the amount of alkali

131   required for maintaining the pH of the feed solution. Since pH significantly affects the

132   ammonia transfer rate across the membrane, more accurate predictions can be achieved

133   with the developed model. For all of that, this model is a useful tool to evaluate the

134   operational costs related to nitrogen recovery process and to optimise it.

135

136   **2.   Material and methods**

137   **2.1. Experimental conditions and set-up.**

138   The set-up for nitrogen recovery used in this work is shown in Figure 1. It consists in

139   two peristaltic pumps, two HFMCs (X50 2.5x8 Liqui-Cel $^{®}$ Extra-flow of PP with a

140   membrane surface of $1.4 m^2$) in series and two reactors of $1.2 \cdot 10^{-3} m^3$, one containing

141   the acid solution (acid tank) and the other one containing the nitrogen rich solution

142   (feed tank). Reactors were closed but not sealed to minimize free ammonia stripping.

143   Each tank was equipped with electronic sensors (Two SP10T, Consort®) in order to

144   measure temperature and pH. Sensors were connected to a multiparametric analyser

145   (Consort C832) which was in turn connected to a PC for data monitoring and storage.

146   Data sampling of pH and temperature was conducted every 20 seconds.
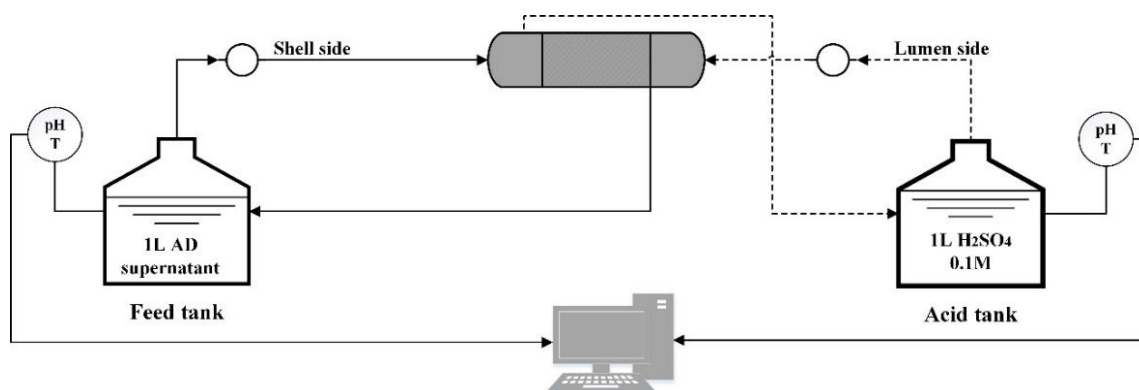
147

148

149 Figure 1. Nitrogen recovery set-up

150 Nitrogen rich solution was pumped through the shell side of HFMCs to avoid the

151 potential fouling due to the larger space available relative to the inside of the much

152 smaller membrane fibre [10]. Acid solution, (H_2SO_4, 0.1M) was pumped counter-

153 currently through the lumen side. Both streams were recycled to their respective

154 reservoirs. A relation of 1:3 between acid solution and nitrogen rich solution flow rates

155 was kept according to membrane manufacturers' recommendations.

156 **2.2. Analytical methods**

157 To characterize the anaerobic digestion supernatant, the following parameters were

158 measured. According to Standard Methods [27], Total Solids (TS (2540B)), Total COD

159 (COD_T (5220B)), Ammonium (NH_4^+-N (4500 NH_3-D)), Phosphate (PO_4^{3-}P(4500P-E))

160 were determined. Ammonium and phosphate were analysed with a photometer

161 SMARTCHEN ® 450 of AMS Alliance. The photometer has the methods mentioned

162 above implemented to be analysed automatically. Thus, Alkalinity and volatile fatty

163 acids concentration were measured by titration according to the methodology proposed

164 by the South African Water Research Commission [28].

165 The experiment monitoring was carried out taking a 3 ml sample of the feed tank to

166 measure the ammonium concentration at different times. For that porpoise, the sample

167 was diluted in a certain volume and analysed in the automatic photometer.

168 **2.3. Nitrogen rich solution**

169 The nitrogen rich solution used in this research is the supernatant from the anaerobic

170 digester of a full scale wastewater treatment plant located in Valencia (Spain). This

171 stream was pre-treated before carrying out the experiments. The pre-treatment consisted

172 in pH adjustment, settling and filtration. Firstly, the pH was increased up to the

173 established value by adding a NaOH solution (1 M). The established pH value varied

174 from 9 to 11 (see table 2) and the amount of NaOH (1M) added varied from 27 to 73

175 ml. When the pH of the anaerobic digestion supernatant was raised, different

176 compounds (mainly calcium phosphate and calcium carbonate) precipitated which were

177 also susceptible of clogging the membrane. To reduce this risk, the solids were settled

178 during 8 minutes and the supernatant was passed through a 0.45 μm filter before feeding

179 the HFMC. For process scale-up a membrane filtration process would be required to

180 protect HFMC modules. Table 1 shows the stream characterization before and after the

181 pre-treatment.

182 Table 1. Anaerobic digestion supernatant characterization before and after the pre-

183 treatment.

Parameter	Before pre-treatment	After pre-treatment
COD (g/m^3)	1320 ± 15	620 ± 22
TSS (g/m^3)	5606 ± 50	< L.D.
NH$_4$-N (g/m^3)	820 ± 180	713 ± 168
PO$_4$-P (g/m^3)	30.5 ± 1.5	2.3 ± 0.8
Alkalinity (g CaCO$_3$/ m^3)	2733.9 ± 31.1	*

pH	8.1	*

*Alkalinity and pH depends on the operating conditions of each experiment (see Table 2)

184

185 **2.4. Experimental procedure**

186 Twenty-five experiments divided into 4 groups were performed in different operating

187 conditions, which are shown in Table 2. The first group consisted in 6 experiments

188 carried out to study the effect of pH over the nitrogen recovery rate. According to

189 Darestani et al [29], pH is the main factor affecting nitrogen recovery with HFMC

190 technology and it should be maintained over 8. Since this statement was previously

191 verified, pH values selected for the experiments were 9, 10 and 11. Although according

192 to the membrane manufacturers there are not operational pH requirements for

193 maintaining the membrane stability, pH values higher than 11 were not evaluated

194 because at this pH all the ammonium nitrogen is present as free ammonia. Furthermore,

195 the higher the pH, the higher the cost of chemical reagents.

196 The second group consisted in four experiments performed to determine the effect of

197 membrane surface over the nitrogen recovery rate and the third group consisted in nine

198 experiments carried out to determine the effect of feed flow rate over the nitrogen

199 recovery rate. Finally, the fourth group of experiments was focused on studying the

200 effect of temperature of the nitrogen rich solution (in the range from 25 to 35ºC) over

201 the nitrogen recovery rate. Temperature of the acid solution was maintained at 25ºC.

202 The duration of the experiments varied from 15 to 80 minutes according to the

203 operating conditions. In each experiment, at regular time intervals, 3 ml samples were

204 taken from the feed tank being diluted to a certain volume for ammonium measurement.

205 The photometer used is able to measure ammonium concentrations between 0.12 and

206 7.89 g N/m^3 so dilutions between 1:150 and 1:5 have been used. Samples from the

207 majority of the experiments were taken at 0', 5', 15',25',40' and 60'. However, in some

208 experiments, the timing was slightly modified because of the different nitrogen recovery

209 rates. Each experimental result reported is the arithmetic mean of at least two replicate

210 measurements. The uncertainty of the analytical method is 3%. Therefore, all the values

211 that deviated more than 3% from the average of the replicates were discarded.

212 Table 2. Operating conditions for the experiments carried out

Groups	Nº	pH	T (ºC)	Membrane surface (m^2)	Feed Flow rate x 10^5 (m^3/s)
1st	1	9	25	1.4	0.67
	2	10	25	1.4	0.67
	3	11	25	1.4	0.67
	4	9	25	2.8	2.50
	5	10	25	2.8	2.50
	6	11	25	2.8	2.50
2nd	7	10	25	1.4	1.00
	8	10	25	2.8	1.00
	9	11	25	1.4	0.33
	10	11	25	2.8	0.33
3rd	11	10	25	2.8	0.33
	12	10	25	2.8	0.67
	13	10	25	2.8	1.00
	14	10	25	2.8	1.67
	15	10	25	2.8	2.50
	16	10	25	2.8	3.34
	17	10	25	2.8	4.17
	18	10	25	2.8	5.00
	19	10	25	2.8	5.83
4th	20	10	25	2.8	4.17
	21	10	30	2.8	4.17
	22	10	35	2.8	4.17
	23	9	25	1.4	1.00
	24	9	30	1.4	1.00
	25	9	35	1.4	1.00

213

214 **2.5. Model development**

215 A mathematical model able to simulate the time evolution of pH and total ammonium

216 nitrogen (TAN) concentration during the nitrogen recovery process has been developed.

217 The following assumptions were made for the model development:

218 • As the HFMCs used were hydrophobic and gas-permeable, it is assumed that the

219   transfer of the aqueous phase through the membrane is restricted.

220 • The high proton concentration of the acid solution leads NH_3 to be immediately

221   converted into NH_4^+. Thus, the mass transfer resistance in the acid solution is

222   negligible.

223 • Temperature and flow rate are constant within the system.

224 • Permeability is considered constant. The nitrogen rich solution pre-treatment and the

225   use of the shell side for this stream minimizes the potential fouling. Furthermore,

226   wetting processes have not been detected at the operating conditions evaluated.

227   Other negative effects for permeability such as concentration polarity are not taking

228   into account.

229

230 **2.5.1. Model Components**

231 Chemically, the system is represented by a set of components and a set of species.

232 Component and species definitions are after Allison et al [30]. These well-known

233 definitions are briefly reviewed here. A species is defined as every chemical entity to be

234 considered. For the set of species selected, a set of components is chosen so that each

235 species can be written as the product of a reaction involving only components, and no

236 component can be written as the product of a reaction involving other components.

237 With this chemical representation, two characteristic variables are defined: the species

238   concentration, C_i (M/L^3), and the components concentration, T_j (M/L^3), being T_j the

239   sum of concentrations of all the species in which this component participates.

240   As commented before, the NH_3 transfer across the membrane modifies the chemical

241   equilibrium between NH_3 and NH_4 increasing the proton concentration. This fact affects

242   all the chemical equilibriums in which the proton is involved (acid base reactions).

243   Therefore, in order to predict the pH evolution, the developed model considers all the

244   components involved in acid base reactions, which are defined as follows:

245   S_{TAN} (g N/m^3): Total ammonium nitrogen. Ammonium plus ammonia nitrogen.

246   S_{PO4} (g P/m^3): Inorganic soluble phosphate, primarily ortophosphates.

247   S_A (g COD/m^3): Acetate plus acetic acid.

248   S_{IC}: Inorganic carbon (mmol C/m^3): This component represents the total

249   inorganic carbon, the analytic sum of $H_2CO_3^*$, HCO_3^- and CO_3^{2-}. This

250   component also includes carbon dioxide which is involved in the following

251   equilibrium:

252
$$CO_2(aq) + H_2O \leftrightarrows H_2CO_3 \text{ (1)}$$

253   The equilibrium for this reaction is moved to the left, and by far the greater fraction of

254   H_2CO_3 is present in the form of CO_2 (aq). As it is difficult analytically to distinguish

255   between CO_2 (aq) and H_2CO_3, $H_2CO_3^*$ is defined as the analytic sum of H_2CO_3 and CO_2

256   (aq) [31]. Inorganic carbon concentration cannot be directly measured and it is

257   calculated from the pH and carbonate alkalinity measurements

258   S_{HT} (kmol H$^+$/m^3): Protons. This component represents the analytic sum of those

259   species in which H$^+$ participates (see Eq. 2).

$$S_H = [H^+] + [HCO_3^-] + 2[H_2CO_3]^* + [HPO_4^{2-}] + 2[H_2PO_4^-] +$$

$$3[H_3PO_4] + [CH_3COOH] - [NH_3] - [OH^-] \quad (2).$$

The species that can be formed from the components mentioned above are listed on the matrix of components-species shown in Table 3.

Table 3. Stoichiometric matrix components-species

Species (C_i)	Components (T_j)					
	H_2O	H^+	NH_4^+	$PO_4{}^{3-}$	$CO_3{}^{2-}$	CH_3COO^-
H_2O	1					
H^+		1				
NH_4^+			1			
$PO_4{}^{3-}$				1		
$CO_3{}^{2-}$					1	
OH^-	1	-1				
NH_3		-1	1			
HCO_3^-		1			1	
H_2CO_3		2			1	
$HPO_4{}^{2-}$		1		1		
$H_2PO_4^-$		2		1		
H_3PO_4		3		1		
CH_3COOH		1				1
CH_3COO^-						1

2.5.2. Model Processes

The structure of the developed model is determined by the time scales of the processes involved:

269   •   Kinetic governed processes: Biochemical processes (reactions) and physical

270   processes (aeration and gas stripping) proceed at a certain rate and are calculated by

271   mass-balance equations. The resulting set of differential equations needs to be

272   integrated over time in order to calculate the gradual change of concentrations.

273   •   Equilibrium governed processes: Acid–base dissociation processes are assumed to

274   happen instantly and are calculated by equilibrium chemistry-based algorithms. In

275   each time step the concentrations of the species are balanced with no effect on the

276   total concentration of the components.

277 The unique kinetic governed process considered is free ammonia stripping across the

278 membrane. It is assumed that free ammonia is the unique gaseous species passing across

279 the membrane and that any biochemical reaction takes place in the feed tank.

280 Furthermore, stripping processes in the feed tank are considered to be negligible since it

281 is closed and low stirring conditions are maintained. However, the proposed model

282 could be easily enlarged including these processes.

283 In the free ammonia stripping process, the stoichiometric coefficient for S_{NH4} is -1 and

284 the stoichiometric coefficient for S_{HT} has been calculated applying continuity equation

285 for proton. The protons content of S_{TAN} is -1/14 and it has been calculated from its

286 stoichiometric formula. The proton content of S_{HT} is -1. Since protons are counted twice

287 this factor must be negative [31].

288 Equation 3 describes the free ammonia stripping rate. Ammonia flux (J) across the

289 membrane depends on the mass transfer coefficient k and the difference between free

290 ammonia concentrations on both sides of the membrane.

291 $$J = k \; x \left(C_{NH3,sh} - C_{NH3,lu} \right) (3)$$

292 where k is the mass transfer coefficient (m/s), $C_{NH3,sh}$ (kg/m^3) is the free ammonia

293 concentration in the shell side (feed solution) and $C_{NH3,lu}$ (kg/m^3) is the concentration in

294 the lumen side (acid solution). $C_{NH3,lu}$ is considered to be negligible.

295 The equilibrium governed processes included in the developed model are the acid base

296 reactions. These reactions are described by a set of nonlinear algebraic equations

297 including one law of mass action for each species (Eq.4) and one mass-balance for each

298 component (Eq.5).

299 $$x_i = K_i \prod_{j=1}^{Nc} x_j^{a_{ij}} \quad i = 1,2 \dots N_{sp} \ (4)$$

300 $$T_j = \sum_{i=1}^{Nsp} a_{ij} C_i \quad j = 1,2 \dots N_c \ (5)$$

301 where x_i is the activity of the *i*th species, a_{ij} is the stoichiometric coefficient of the *j*th

302 component in the *i*th species, K_i is the stability constant of the *i*th species corrected for

303 temperature variations and T_j is the concentration of the component and C_i is the

304 concentration of the species. Nsp is the number of species included in the model and Nc

305 is the number of components.

306 **2.5.3. Model implementation**

307 The developed model was implemented in MATLAB – Simulink$^©$ for dynamic

308 simulations. The concentration of every species present in equilibrium is calculated

309 using MINTEQA2 [30]. MINTEQA2 is a program developed by USEPA including a

310 geochemical equilibrium speciation model capable of computing equilibria among the

311 dissolved, adsorbed, solid and gas phases. MINTEQA2 original code has been slightly

312 modified and compiled through the dynamic link library (DLL), techniques allowing the

313 FORTRAN module to be linked promptly to MATLAB – Simulink$^©$.

314 The solution procedure consists in an iterative process. For each time step, mass

315 balances are calculated obtaining the concentration of each component. After that,

316 MINTEQA2 calculates the equilibrium composition obtaining the concentration of each

317 species. The iterative process for each simulation ends when the maximum simulation

318 time is reached.

2.5.4. Model application

Mass Balances in the feed tank

321 Since the unique kinetic governed process considered is ammonia stripping across the

322 membrane the concentration of all the model components in the feed tank except S_{TAN}

323 and S_{HT} will remain constant. Equations 6 and 7 represent the mass balance equation

324 applied for these components. Furthermore, the mass balance scheme is added as

325 Supplementary Data.

326 $$Q \times S_{TANoutput} - Q \times S_{TANinput} + V \times \frac{dS_{TAN}}{dt} = 0 \ (6)$$

327 $$Q \times S_{HToutput} - Q \times S_{HTinput} + V \times \frac{dS_{HT}}{dt} = 0 \ (7)$$

328 where $S_{TANinput}$ and $S_{HTinput}$ represent the TAN concentration and the total proton

329 concentration returning to the feed tank from the HFMC, respectively. $S_{TANoutput}$ and

330 $S_{HToutput}$ are the TAN concentration and total proton concentration in the feed tank,

331 respectively, since feed tank is assumed to be a continuous stirred tank reactor. V is the

332 volume of the feed tank and Q is the feed flow rate

333 When solving the differential equations, for each time step the concentrations of each

334 species are calculated using Eq. 4 and Eq. 5.

Mass balances in the HFMC

336 Free ammonia concentration and pH decrease when nitrogen rich stream circulates

337 along the shell side. In order to obtain an accurate prediction for free ammonia mass

338 transfer the HFMC is divided into 10 subunits as a plug flow reactor (see

16

339   Supplementary Data). The number of subunits was established in accordance with

340   Abusam and Keesman [32]. Equations 8 and 9 show the mass balances applied for S_{TAN}

341   and S_{HT} in each subunit of the HFMC.

342    $$Q \times S_{TAN_i} - Q \times S_{TAN_{i-1}} + V \times \frac{dS_{TAN_i}}{dt} = k \times A \times S_{NH3_i} \quad i = 1,2\dots 10 \ (8)$$

343    $$Q \times S_{HT_i} - Q \times S_{HT_{i-1}} + V \times \frac{dS_{HT_i}}{dt} = k \times A \times \frac{S_{NH3_i}}{14} \quad i = 1,2\dots 10 \ (9)$$

344   Where S_{TANi} and S_{HTi} represents the TAN concentration and proton concentration in the

345   subunit i. Subunit 0 corresponds to the stream entering the HFMC, whose

346   concentrations are those calculated for the feed tank. Concentrations in the stream

347   exiting from the HFMC are those calculated for the subunit 10 (the last one). A is the

348   membrane surface and k is the mass transfer coefficient.

349   When solving the differential equations in each subunit, for each time step the

350   concentrations of each species are calculated using Eq. 4 and Eq. 5. Model parameters

351   were determined carrying out the required simulations in MATLAB – Simulink$^{©}$ for

352   minimizing the residual sum of squared errors between the experimental data and the

353   model predictions.

354   **3. Results and discussion**

355   **3.1. Experimental results**

356   TAN concentration in the acid tank was measured only at the end of each experiment.

357   The recovery efficiency achieved in all the experiments was around 99%. Nitrogen

358   losses by stripping were not observed during the experiments.

359   **3.1.1. First group of experiments: pH effect on nitrogen recovery rate**

360   Figure 2a and Figure 2b show the time evolution of TAN concentration in the feed tank

361   (C/C$_0$) observed in experiments 1-3 and 4-6 respectively. As can be seen on these

362   figures, complete ammonium removal is achieved in all the experimental conditions

363 evaluated but nitrogen recovery rate depends on the pH value. The higher the pH, the

364 higher the recovery rate. This trend can be observed in both figures despite the different

365 feed flow rate and membrane surface between experiments represented.
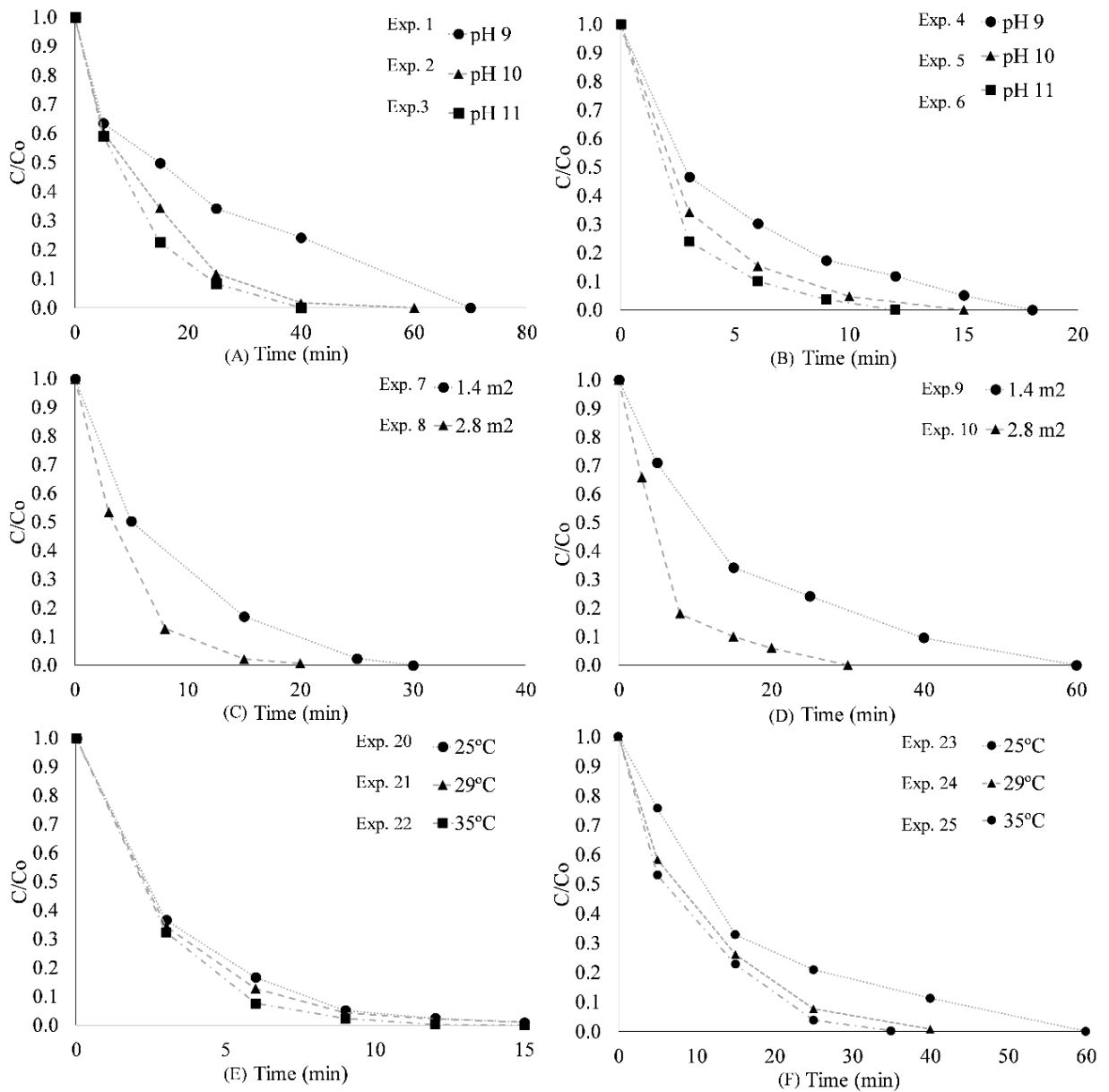
366

367 Figure 2. Time evolution of TAN concentration for: a) experiments 1-3 b) experiments

368 4-6 c) experiments 7-8, d) experiments 9-10, e) experiments 20-22 f) experiments 23-25

369

370   These results are in accordance with those reported by Ashrafizadeh and Khorasani

371   [21] and Kartohardjono et al [33]. The effect of pH on nitrogen recovery rate is related

372   to the percentage of TAN present as free ammonia (at T=25ºC, 36% at pH 9, 85% at pH

373   10, and 98% at pH 11, see Figure 3). Because of that, the difference in nitrogen

374   recovery rate between the experiments carried out at pH 9 and 10 is higher than the

375   difference observed between the experiments carried out at pH 10 and 11.
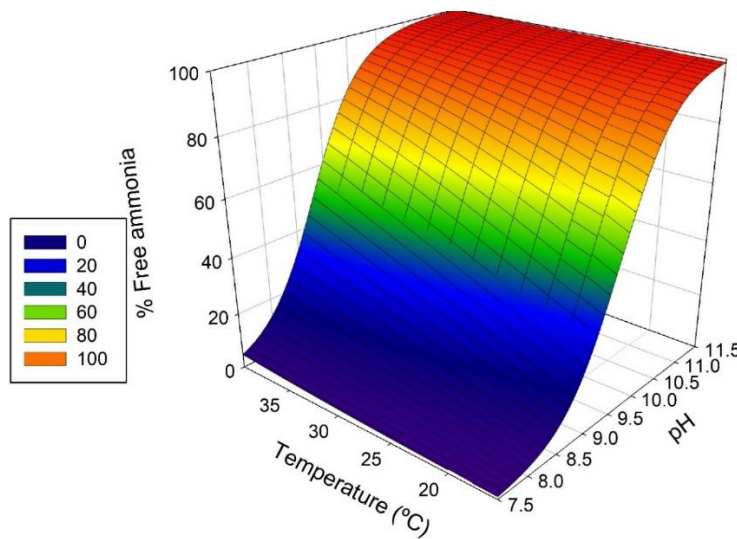
376

377   Figure 3. Free ammonia percentage vs pH and temperature

378   **3.1.2.   Second group of experiments: membrane surface effect on nitrogen**
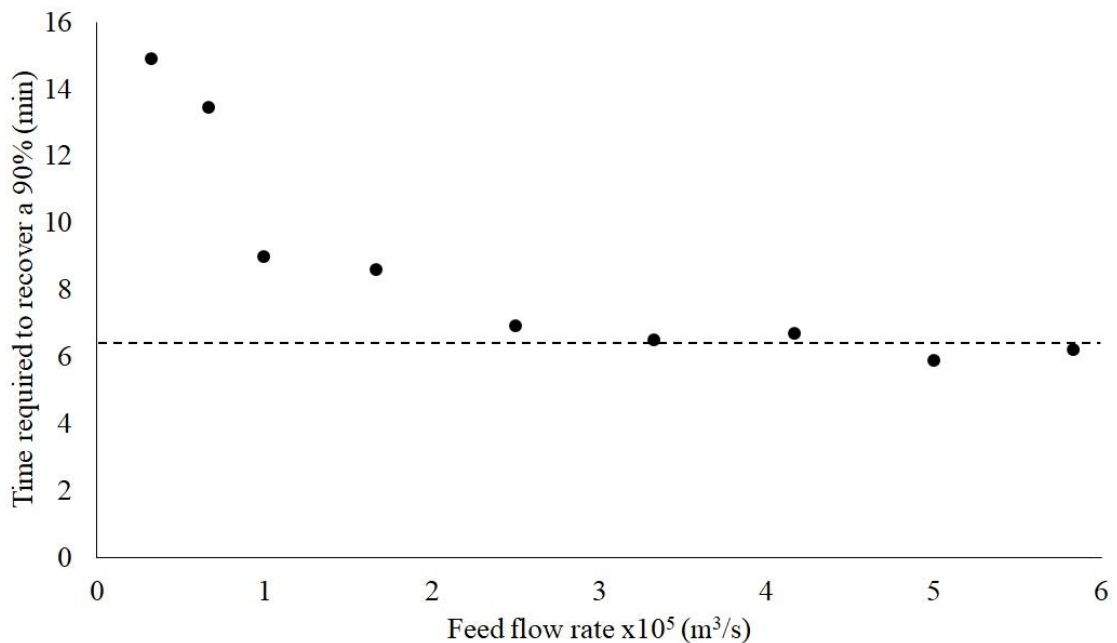
379   **recovery rate**

380   Figure 2c and figure 2d show the time evolution of TAN concentration in the feed tank

381   (C/C$_0$) observed in experiments 7-8 and 9-10, respectively. As can be seen in these

382   figures, in the experiments carried out with one HFMC (A=1.4m^2; Exp 7-8) the time

383   required for recovering a given percentage of nitrogen is twice the time required in the

384   experiments carried out with two HFMC (A=2.8m^2; Exp 9-10). This result can be

385   observed in both figures despite the different feed flow rate and pH of the experiments.

386 It indicates that the effectiveness of both membranes in series is the same, so all the

387 surface was used, and that the best configuration is two HFMC in series.

388 **3.1.3. Third group of experiments: feed flow rate effect on nitrogen recovery rate.**

389 As commented before, experiments 11-19 were carried out with the same operating

390 conditions except for the feed flow rate. Figure 4 shows the time required to achieve a

391 90% nitrogen recovery efficiency as a function of the feed flow rate. As can be seen in

392 this figure, the required time decreased when the feed flow rate was increased.

393 However, it remained constant for flow rates higher than 2.5×10^{-5} m^3/s. Thus, this value

394 is the optimum feed flow rate, since higher values lead to higher pumping energy costs

395 without increasing ammonia recovery rate. The turbulence created inside the HFMCs at

396 high feed flow rates removes the boundary layer leading to a constant transfer rate

397 across the membrane. Liu and Wang [34] also observed that the ammonia transfer rate

398 was increased when increasing the feed flow rate but it tended to an asymptotic value.

399

400 Figure 4. Time required to achieve a 90% nitrogen recovery efficiency at different feed

401 flow rates.

402

3.1.4. Fourth group of experiments: temperature effect on nitrogen recovery rate

404 Figure 2e and figure 2f show the time evolution of TAN concentration in the feed tank

405 (C/C_0) observed in experiments 20-22 and 23-25, respectively. It can be seen in both

406 figures that the higher the temperature in the feed tank, the higher the nitrogen recovery

407 rate. High temperatures increase the percentage of TAN present as free ammonia.

408 However, the effect of temperature is more significant at low pH values. It can be

409 explained because the percentage of free ammonia also depends of pH value (see Figure

410 3). In the experiments 20-22 carried out at pH 10, the percentage of free ammonia

411 reached the 85% at 25ºC, and it slightly increased up to 89% and 92% at 30ºC and 35ºC,

412 respectively. However, in the experiments 23-25 carried out at pH 9, the percentage of

413 free ammonia was 36% at 25ºC, and sharply increased up to a 44% and 53% at 30 ºC

414 and 35ºC, respectively. The results obtained indicate than the higher the pH, the less

415 important the temperature effect on nitrogen recovery rate.

3.2. Model validation

417 The time evolution of TAN concentration in the feed tank measured in the different

418 experiments has been compared with model predictions obtained with equation 10.

419
$$S_{TANt+\Delta t} = S_{TANt} - \left(\frac{Q \cdot \Delta t \cdot (S_{TANt} - S_{TAN10})}{V}\right) \text{ (10)}$$
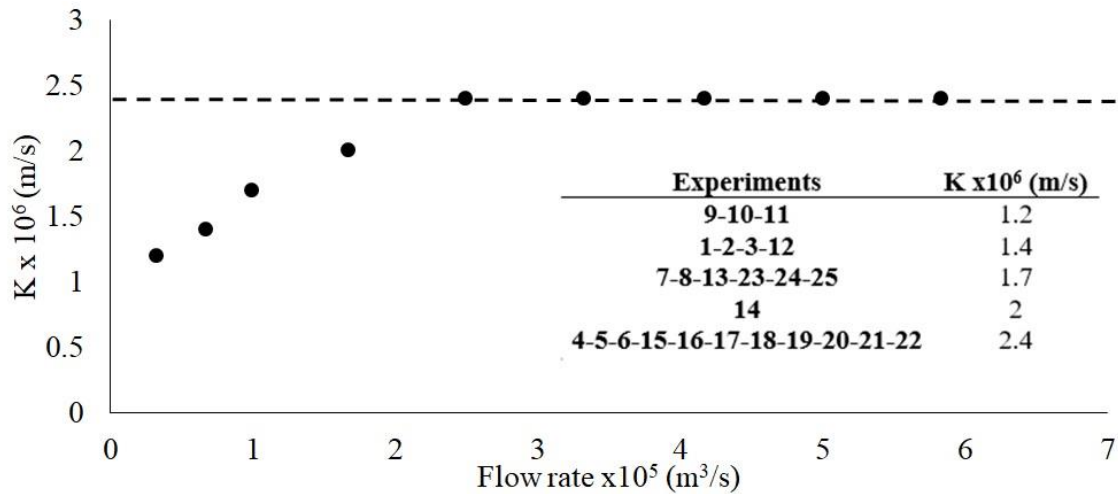
420 where S_{TAN10} represents the TAN concentration recycled to the feed tank from the

421 membrane contactor and it is calculated with equation 11

422
$$S_{TAN_i} = S_{TAN_{i-1}} - \left(\frac{k \cdot A \cdot S_{NH3_{i-1}}}{Q}\right) \quad \text{i (membrane subunit)} = 1,2,3...10 \quad \text{(11)}$$

423   Free ammonia concentration required for applying equation 11 is obtained with the

424   chemical governed process considered (eq 4 and 5) and the mass balance for total

425   proton concentration.

426   In the simulation of all the experiments, at each time step the developed model predicts

427   a significant difference in TAN concentration and pH between the streams entering

428   (subunit 0) and exiting (subunit 10) from the HFMC. These variations reduce the free

429   ammonia concentration (i.e. in the first time step of experiment 4 it decreased from

430   192.4 to 166.2 g N-NH$_3$/ m^3) and the free ammonia stripping rate along the membrane.

431   Because of that, simulations have been carried out dividing the HFMCs in 10 subunits.

432   Dynamic calibration of the model was done by adjusting model predictions to

433   experimental data. Calibration variables were TAN concentration and pH. Free

434   ammonia mass transfer coefficient was gradually changed to minimize the sum of

435   squared relative deviations of the concentration profiles obtained from simulation and

436   those from measurements. Accurate model predictions could not be achieved using the

437   same mass transfer coefficient for all the experiments. The mass transfer coefficient

438   resulted to be dependent on feed flow rate as it was expected because convection is not

439   included in the model. Those experiments carried out with feed flow rates higher than

440   2.5x10^{-5} m^3/s could be accurately reproduced with a mass transfer coefficient of 2.4x10^{-}

441   ^{6} m/s. However, for the experiments with feed flow rates lower than 2.5x10^{-5} m^3/s, the

442   lower the feed flow rate, the lower the mass transfer coefficient obtained. Figure 5

443   shows the mass transfer coefficients obtained for all the experiments.

Figure 5. Mass transfer coefficients obtained at different feed flow rates

Experiments	K x10^6 (m/s)
9-10-11	1.2
1-2-3-12	1.4
7-8-13-23-24-25	1.7
14	2
4-5-6-15-16-17-18-19-20-21-22	2.4

When decreasing the feed flow rate, the boundary layer becomes larger decreasing the

free ammonia concentration near the membrane. Since the developed model

overestimates the free ammonia concentration in the shell side ($C_{NH3,sh}$ in Eq. 3)

because it does not consider the boundary layer formation, the mass transfer coefficients

obtained were lower than those obtained at high feed flow rates. These results are in

accordance with those obtained by Ashrafizadeh and Khorasani [15].

Table 4 shows the comparison of the mass transfer coefficients obtained in this work

with literature values. As can be seen in this table, the values obtained in this work are

similar to those obtained by Kartohardjono et al [33], using the same membrane

contactors. Other authors [21,34,35] reported overall mass transfer quite higher than the

value obtained in this research. However, these authors calculated the mass transfer

considering the total ammonium nitrogen concentration, without taking into account the

free ammonia concentration. This difference leads to an overestimation of the mass

transfer coefficient in comparison with the values obtained in this work. Moreover,

other authors [22,36] using PVDF membrane contactors also reported mass transfer

coefficients higher than the ones obtained in this study. Zhu et al [37] included a term

462 considering the fraction of TAN present as free ammonia. However, it is a fixed value

463 so it cannot reproduce the changes along the experiment when the pH is not maintained.

464 Because of that, the values reported by Zhu et al [37] are higher than the ones presented

465 in this paper.

466 Table 4. Literature values for ammonia mass transfer coefficients in HFMC.

Mass transfer coefficient (m/s)	Reference
$1.2\text{-}2.4 \times 10^{-6}$	This work
$0.1\text{-}1.4 \times 10^{-5}$	[21]
$2.0\text{-}6.0 \times 10^{-5}$	[36]
$1.0\text{-}2.5 \times 10^{-4}$	[35]
$0.5\text{-}1.5 \times 10^{-6}$	[33]
$0.1\text{-}1.5 \times 10^{-6}$	[22]
$0.1\text{-}1.4 \times 10^{-5}$	[37]
$5.3\text{-}8.9 \times 10^{-6}$	[34]

467

468 Figure 6a and Figure 6b show the accuracy of the model predictions for TAN

469 concentration and pH comparing the experimental values determined for all the

470 experiments with the simulated ones. As can be seen in these figures, the correlation

471 factor is close to 1 demonstrating that the developed model is able to accurately

472 simulate the time evolution of TAN concentration and pH in all the experiments

473 regardless the different pH, flow rates, membrane surface and temperature.

474 The evolution of pH and TAN concentration in experiments 4-6 (carried out at different

475 pH values), 11-19 (carried out at different feed flow rates) and 20-22 (carried out at

476 different temperatures) jointly with model predictions is included as Supplementary

477 Data. Despite the different pH values in experiments 4, 5 and 6, the developed model

478 accurately reproduced with the same mass transfer coefficient the experimental values

479 obtained in these experiments. Ashrafizadeh and Khorasani [15] and Qu et al [28]

480 reported a mass transfer coefficient affected by the pH, but these authors considered that

481 the ammonia stripping rate depended on TAN concentration. Considering the free

482 ammonia concentration (Eq. 3) calculated with the acid base reactions (Eq. 4 and Eq.5)

483 the mass transfer coefficient does not depend on pH. In the same way, experiments 20-

484 22 could be reproduced with the same mass transfer coefficient because the developed

485 model considers that ammonia transfer rate depends on free ammonia concentration,

486 which increases at high temperatures. Regarding to experiments 11-19, the experiment

487 with the lowest flow rate evaluated (exp. 11) lasted 30 minutes for complete ammonium

488 removal. This time was reduced to 15 minutes in the experiment carried out at the

489 highest flow rate evaluated (exp. 19). The model developed in this research accurately

490 reproduced the experimental results for all the feed flow rates evaluated, but as

491 commented before, with different mass transfer coefficients due to the boundary layer

492 formation at low flow rates.
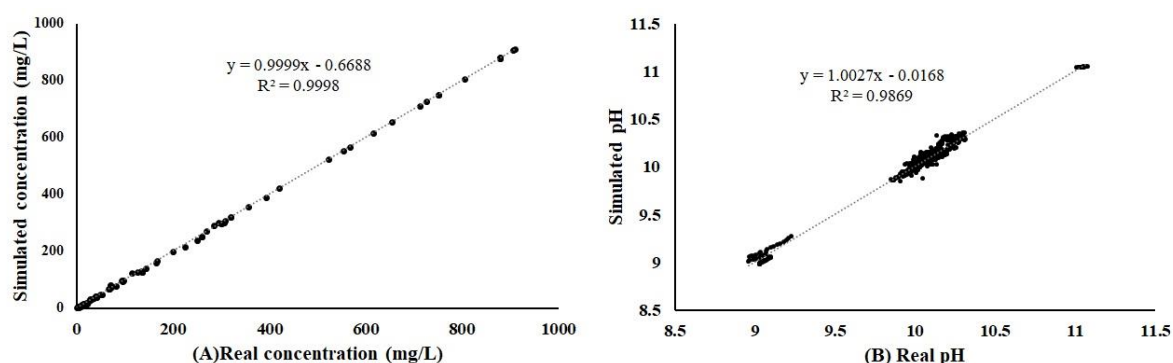
493

494 Figure 6. Model predictions vs experimental results for: a) TAN concentration b) pH.

495 The slight pH increments that can be observed during most of the experiments are due

496 to NaOH additions required to maintain the pH in the feed tank. To simulate these

497 NaOH additions, the moles of OH$^-$ added were estimated taking into account the

498   volume of NaOH added (recorded by the pH controller), as well as the purity and

499   density of the NaOH solution. The moles of OH^- added are substracted from the S_{HT}

500   concentration in the feed tank.

501   In order to evaluate the model capability to represent pH variations higher than the

502   observed in the aforementioned experiments, one last experiment was carried out

503   without controlling the pH in the feed tank, therefore, NaOH was not added during this

504   experiment. As a consequence, pH decreased from 9.0 to 8.1 due to the ammonia

505   transfer across the membrane. Nitrogen recovery rate decreased due to the low pH

506   values reached, and the process was nearly stopped at pH around 8.5. In the first five

507   minutes TAN concentration decreased 63 g N/ m^3, but between t=15min and t=25 min

508   TAN concentration only decreased 22 g N/ m^3. These results are in accordance with

509   those obtained by Darestani et al [8]. The developed model accurately reproduced the

510   pH decrease as well as the evolution of TAN concentration during this experiment. The

511   evolution of pH and TAN concentration jointly with model predictions is included as

512   Supplementary Data.

513   According to the results obtained, the most important factors affecting nitrogen recovery

514   rate are the nitrogen rich solution flow rate and pH. Low flow rates decrease the mass

515   transfer coefficient due to the boundary layer formation and pH determines the free

516   ammonia concentration. Temperature also affects the free ammonia concentration but

517   its effect is less significant than pH effect. Furthermore, it should be highlighted that

518   since the proposed model considers that free ammonia transfer rate depends on the

519   difference between free ammonia concentrations on both sides of the membrane the

520   effect of pH and temperature is included intrinsically. Modelling pH evolution allows

521   considering the free ammonia concentration instead of TAN, which increases the

522   accuracy of model predictions. The developed model is a useful tool for process design,

523 since it can predict the time required for reaching the desired nitrogen recovery

524 efficiency and the amount of NaOH required to maintain the pH in the feed tank.

525 **4. Future scale-up development**

526 The results obtained in this work are very useful in different aspects for optimizing

527 future full scale implementations of these technology. On the one hand, the pretreatment

528 should be studied in depth to reduce process costs and nitrogen losses. Around the 15

529 %w/w of the nitrogen was lost during the pretreatment carried out in the laboratory

530 experiments. On the other hand, the mathematical model developed could be a useful

531 tool for determining the membrane surface required since model predictions provide the

532 time required for achieving the removal percentage desired. Finally, it has been proved

533 that free ammonia transfer rate is directly proportional to the mass transfer coefficient

534 and the free ammonia concentration. Mass transfer coefficient depends on nitrogen rich

535 solution flow rate. For process optimization, this flow rate should be high enough to

536 avoid boundary layer formation; in the case studied, it should be higher than 2.5×10^{-5}

537 m/s. Regarding the free ammonia concentration, it depends on pH and temperature,

538 being the effect of pH more significant than the effect of temperature (see Figure 3). As

539 a matter of fact, at pH values higher than 11.5 the effect of temperature is negligible

540 since all the ammonium nitrogen is present as free ammonia. The higher the pH or the

541 higher the temperature the higher the ammonia transfer rate and, therefore, the lower the

542 membrane surface required. However, increasing the pH or increasing the temperature

543 of the nitrogen rich solution raises the process costs. For process optimization, an

544 economical study should be carried out case by case. This economical study should

545 consider the costs of the membrane and the chemical reagents required as well as the

546 energy required for increasing the temperature. The amount of chemical reagents

547 required that can be estimated with the developed model will depend on the pH value

548 selected and the characteristics of the nitrogen rich stream such as initial pH, alkalinity

549 and total ammonium concentration. A software including the proposed mathematical

550 model and able to carry out these economic analysis taking into account simulation

551 results would be required for full-scale process design and optimization.

552 **5. Conclusions**

553 The main conclusions obtained are:

554 • Nitrogen recovery efficiency close to 100% can be achieved with HFMCs in

555   different operating conditions.

556 • Nitrogen recovery rate depends on membrane surface available, feed flow rate and

557   NH_3 concentration, which in turn depends on pH and temperature. However, pH is

558   the most important factor.

559 • The developed model accurately reproduced ($R^2 > 0.98$) the time evolution of pH and

560   TAN concentrations in 26 experiments predicting the NaOH required to control the

561   pH in the feed tank.

562 • The mass transfer coefficient obtained does not depend on pH or temperature. It was

563   only affected by the boundary layer formed at low feed flow rates. The value

564   obtained at high flow rates was 2.4×10^{-6} m/s.

565 E-supplementary data of this work can be found in online version of the paper

7. References

[1] L.F. Razon, Life cycle analysis of an alternative to the haber-bosch process: Non-renewable energy usage and global warming potential of liquid ammonia from cyanobacteria, Environ. Prog. Sustain. Energy. 33 (2014) 618–624. doi:10.1002/ep.11817.

[2] Z. Guo, Y. Sun, S.-Y. Pan, P.-C. Chiang, Integration of Green Energy and Advanced Energy-Efficient Technologies for Municipal Wastewater Treatment Plants, Int. J. Environ. Res. Public Health. 16 (2019) 1282. doi:10.3390/ijerph16071282.

[3] D.J. Batstone, T. Hülsen, C.M. Mehta, J. Keller, Platforms for energy and nutrient recovery from domestic wastewater: A review, Chemosphere. 140 (2015) 2–11. doi:10.1016/j.chemosphere.2014.10.021.

[4] D. Puyol, D.J. Batstone, T. Hülsen, S. Astals, M. Peces, J.O. Krömer, Resource Recovery from Wastewater by Biological Technologies: Opportunities, Challenges, and Prospects., Front. Microbiol. 7 (2016) 2106. doi:10.3389/fmicb.2016.02106.

[5] N. Martí, R. Barat, A. Seco, L. Pastor, A. Bouzas, Sludge management modeling to enhance P-recovery as struvite in wastewater treatment plants, J. Environ. Manage. 196 (2017) 340–346. doi:10.1016/j.jenvman.2016.12.074.

[6] D. Aguado, R. Barat, A. Bouzas, A. Seco, J. Ferrer, P-recovery in a pilot-scale struvite crystallisation reactor for source separated urine systems using seawater and magnesium chloride as magnesium sources, Sci. Total Environ. 672 (2019) 88–96. doi:10.1016/j.scitotenv.2019.03.485.

594   [7]   X. Zhang, J. Hu, H. Spanjers, J.B. van Lier, Struvite crystallization under a

595   marine/brackish aquaculture condition, Bioresour. Technol. (2016).

596   doi:10.1016/j.biortech.2016.07.088.

597   [8]   Á. Robles, D. Aguado, R. Barat, L. Borrás, A. Bouzas, J.B. Giménez, N. Martí, J.

598   Ribes, M.V. Ruano, J. Serralta, J. Ferrer, A. Seco, New frontiers from removal to

599   recycling of nitrogen and phosphorus from wastewater in the Circular Economy,

600   Bioresour. Technol. (2020). doi:10.1016/j.biortech.2019.122673.

601   [9]   C. Vaneeckhaute, V. Lebuf, E. Michels, E. Balia, P.. Vanrolleghem, F.M.. TAck,

602   E. Meers, Nutrient Recovery from Digestate: Systematic Technology Review and

603   Product Classification, Waste Biomass Valorization. 8 (2017) 21–40.

604   doi:10.1007/s12649-016-9642-x.

605   [10]   M. Darestani, V. Haigh, S.J. Couperthwaite, G.J. Millar, L.D. Nghiem, Hollow

606   fibre membrane contactors for ammonia recovery: Current status and future

607   developments, J. Environ. Chem. Eng. 5 (2017) 1349–1359.

608   doi:10.1016/j.jece.2017.02.016.

609   [11]   S. Daguerre-Martini, M.B. Vanotti, M. Rodriguez-Pastor, A. Rosal, R. Moral,

610   Nitrogen recovery from wastewater using gas-permeable membranes: Impact of

611   inorganic carbon content and natural organic matter, Water Res. 137 (2018) 201–

612   210. doi:10.1016/j.watres.2018.03.013.

613   [12]   M. Younas, S. Druon Bocquet, J. Sanchez, Extraction of aroma compounds in a

614   HFMC: Dynamic modelling and simulation, J. Memb. Sci. (2008).

615   doi:10.1016/j.memsci.2008.06.045.

616   [13]   D. Qiu, Z. Wu, S.M. Huang, W.B. Ye, X. Chen, J. Luo, M. Yang, Laminar flow

617   and heat transfer in an internally-cooled hexagonal parallel-plate membrane

618   channel (IHPMC), Appl. Therm. Eng. (2017).

619   doi:10.1016/j.applthermaleng.2017.06.079.

620   [14]   A. Seco, S. Aparicio, J. González-Camejo, A. Jiménez-Benítez, O. Mateo, J.F.

621   Mora, G. Noriega-Hevia, P. Sanchis-Perucho, R. Serna-García, N. Zamorano-

622   López, J.B. Giménez, A. Ruiz-Martínez, D. Aguado, R. Barat, L. Borrás, A.

623   Bouzas, N. Martí, M. Pachés, J. Ribes, A. Robles, M. V. Ruano, J. Serralta, J.

624   Ferrer, Resource recovery from sulphate-rich sewage through an innovative

625   anaerobic-based water resource recovery facility (WRRF), Water Sci. Technol.

626   78 (2018) 1925–1936. doi:10.2166/wst.2018.492.

627   [15]   M.C. Garcia-González, M.B. Vanotti, Recovery of ammonia from swine manure

628   using gas-permeable membranes: Effect of waste strength and pH, Waste Manag.

629   38 (2015) 455–461. doi:10.1016/j.wasman.2015.01.021.

630   [16]   H. Li, W. Wang, Y. Zhang, Preparation and characterization of high-selectivity

631   hollow fiber composite nanofiltration membrane by two-way coating technique,

632   J. Appl. Polym. Sci. 131 (2014) 41187. doi:10.1002/app.41187.

633   [17]   Z. Wang, H. Gong, Y. Zhang, P. Liang, K. Wang, Nitrogen recovery from low-

634   strength wastewater by combined membrane capacitive deionization (MCDI) and

635   ion exchange (IE) process, Chem. Eng. J. 316 (2017) 1–6.

636   doi:10.1016/j.cej.2017.01.082.

637   [18]   L. Richter, M. Wichern, M. Grömping, U. Robecke, J. Haberkamp, Nitrogen

638   Recovery from Process Water of Digested Sludge Dewatering with Membrane

639   Contactors, in: 3rd IWA Resour. Recover. Conf., Venize, 2019: pp. 13–14.

640   [19]   B. Wett, G. Nyhuis, I. Takács, S. Murthy, Development of Enhanced

641   Deammonification Selector, Proc. Water Environ. Fed. 2010 (2012) 5917–5926.

642   doi:10.2175/193864710798194139.

643   [20]   S.R. Wickramasinghe, M.J. Semmens, E.L. Cussler, Hollow fiber modules made

644   with hollow fiber fabric, J. Memb. Sci. 84 (1993) 1–14. doi:10.1016/0376-

645   7388(93)85046-Y.

646   [21]   S.N. Ashrafizadeh, Z. Khorasani, Ammonia removal from aqueous solutions

647   using hollow-fiber membrane contactors, Chem. Eng. J. 162 (2010) 242–249.

648   doi:10.1016/j.cej.2010.05.036.

649   [22]   X. Tan, S.P. Tan, W.K. Teo, K. Li, Polyvinylidene fluoride (PVDF) hollow fibre

650   membranes for ammonia removal from water, J. Memb. Sci. 271 (2006) 59–68.

651   doi:10.1016/j.memsci.2005.06.057.

652   [23]   G.K. Agrahari, S.K. Shukla, N. Verma, P.K. Bhattacharya, Model prediction and

653   experimental studies on the removal of dissolved NH 3 from water applying

654   hollow fiber membrane contactor, J. Memb. Sci. 390–391 (2011) 164–174.

655   doi:10.1016/j.memsci.2011.11.033.

656   [24]   F. Nosratinia, M. Ghadiri, H. Ghahremani, Mathematical modeling and

657   numerical simulation of ammonia removal from wastewaters using membrane

658   contactors, J. Ind. Eng. Chem. 20 (2014) 2958–2963.

659   doi:10.1016/j.jiec.2013.10.065.

660   [25]   E. Licon, M. Reig, P. Villanova, C. Valderrama, O. Gibert, J.L. Cortina,

661   Ammonium removal by liquid–liquid membrane contactors in water purification

662   process for hydrogen production, Desalin. Water Treat. 56 (2015) 3607–3616.

663   doi:10.1080/19443994.2014.974216.

664   [26]   J. Nagy, J. Kaljunen, A.J. Toth, Nitrogen recovery from wastewater and human

665   urine with hydrophobic gas separation membrane: experiments and modelling,

666   Chem. Pap. 73 (2019) 1903–1915. doi:10.1007/s11696-019-00740-x.

667   [27]   American Public Health Association, Standard Methods for the Examination of

668   Water and Wastewater, 19th editi, 1995.

669   [28]   R.E. Moosbrugger, M.C. Wentzel, G.A. Ekama, G. v. R. Marais, A 5 pH Point

670   Titration Method for Determining the Carbonate and SCFA Weak Acid/Bases in

671   Anaerobic Systems, Water Sci. Technol. 28 (1993) 237–245.

672   doi:10.2166/wst.1993.0112.

673   [29]   M. Darestani, V. Haigh, S.J. Couperthwaite, G.J. Millar, L.D. Nghiem, Hollow

674   fibre membrane contactors for ammonia recovery: Current status and future

675   developments, J. Environ. Chem. Eng. 5 (2017) 1349–1359.

676   doi:10.1016/J.JECE.2017.02.016.

677   [30]   J. Allison, D. S. Brown, K. J. Novo-Gradac, MINTEQA2/PRODEFA2, a

678   geochemical assessment model for environmental systems: Version 3. 0 user's

679   manual, GA US Environ. Prot. Agency. (1991).

680   [31]   J. Serralta, J. Ferrer, L. Borrás, A. Seco, An extension of ASM2d including pH

681   calculation, Water Res. 38 (2004) 4029–4038. doi:10.1016/j.watres.2004.07.009.

682   [32]   A. Abusam, K.J. Keesman, Effect of number of CSTR's on the modelling of

683   oxidation ditches: steady state and dynamic analysis., Med. Fac. Landboux. Univ.

684   Gent. 65 (1999) 91–94.

685   [33]   S. Kartohardjono, M. Iwan Fermi, Y. Yuliusman, K. Elkardiana, A. Putra

686   Sangaji, A. Maghfirwan Ramadhan, The Removal of Dissolved Ammonia from

687   Wastewater through a Polypropylene Hollow Fiber Membrane Contactor, Int. J.

688   Technol. 6 (2015) 1146. doi:10.14716/ijtech.v6i7.1845.

689   [34]   H. Liu, J. Wang, Separation of ammonia from radioactive wastewater by

690   hydrophobic membrane contactor, Prog. Nucl. Energy. 86 (2016) 97–102.

691   doi:10.1016/j.pnucene.2015.10.011.

692   [35]   J.-M. Zheng, Z.-W. Dai, F.-S. Wong, Z.-K. Xu, Shell side mass transfer in a

693   transverse flow hollow fiber membrane contactor, J. Memb. Sci. 261 (2005) 114–

694   120. doi:10.1016/j.memsci.2005.02.035.

695   [36]   D. Qu, D. Sun, H. Wang, Y. Yun, Experimental study of ammonia removal from

696   water by modified direct contact membrane distillation, Desalination. 326 (2013)

697   135–140. doi:10.1016/j.desal.2013.07.021.

698   [37]   Z. Zhu, Z. Hao, Z. Shen, J. Chen, Modified modeling of the effect of pH and

699   viscosity on the mass transfer in hydrophobic hollow fiber membrane contactors,

700   J. Memb. Sci. 250 (2005) 269–276. doi:10.1016/j.memsci.2004.10.031.

701